International Journal of Innovative
Computing, Information and Control
Volume 8, Number 6, June 2012

ICIC International ©2012 ISSN 1349-4198
pp. 4299–4318

SELECTION OF PROPER ACTIVATION FUNCTIONS IN BACK-PROPAGATION NEURAL NETWORKS ALGORITHM FOR IDENTIFYING THE PHASE WITH FAULT APPEARANCE IN TRANSFORMER WINDINGS

Atthapol Ngaopitakkul and Chaiyan Jettanasen

Faculty of Engineering
King Mongkut's Institute of Technology Ladkrabang
Chalongkrung Rd., Ladkrabang, Bangkok 10520, Thailand
knatthap@kmitl.ac.th

Received March 2011; revised August 2011

Abstract. *This paper presents an algorithm based on a combination of Discrete Wavelet Transforms and back-propagation neural networks for identifying the types of fault including the phase with fault appearance of a two-winding three-phase power transformer. Fault conditions of the transformer are simulated using ATP/EMTP in order to obtain current signals. The training process for the neural network and fault diagnosis decision are implemented using toolboxes on MATLAB. Various cases and fault types based on Thailand electricity transmission and distribution systems are studied to verify the validity of the algorithm. Various activation functions in each hidden layer and the output layer are compared in order to select the best activation function for identifying the types of internal fault of the transformer winding. It is found that average accuracy obtained from hyperbolic tangent – hyperbolic tangent – linear activation function gives satisfactory accuracy, and will be particularly useful in the development of a modern differential relay.*

Keywords: Wavelet transform, Transformer windings, Neural network, Internal fault

1. **Introduction.** Power transformer is one of the most important pieces of equipment of the power system. When fault occurs in power transformer, detecting fault is necessary in order to clear fault before reaching a level that can damage the power transformer. Conventional methods are still utilized for fault diagnosis for the power transformer employed in Electricity Generating Authority of Thailand (EGAT) such as Dissolved Gas Analysis (DGA) and Measurement winding impedance of transformer method. However, both methods have advantages and disadvantages. Dissolved Gas Analysis (DGA) can detect other fault conditions such as partial discharge (or corona) thermal, but it cannot identify phase and locate the fault taking place in the transformer. On the other hand, a large amount of uncertainty and vagueness would exist in the data for the diagnostic. The measurement of transformer winding impedance has been used by EGAT in the field test because it is not complicated. This method can identify phase and locate fault within transformer. However, it cannot detect other fault conditions. Generally, power transformers can be protected by over-current relays, pressure relays and differential relays depending on purposes [1]. The differential principle, as applied for protecting power transformers, can be illustrated in Figure 1. If an internal fault occurs, the differential current would be simply a very large fault current. It can be easily seen that this is a very powerful discriminator between external and internal faults. However, there are some factors that can cause a needless operation of the differential protection, such as effects from magnetizing inrush current, the current transformers saturation or their ratios that

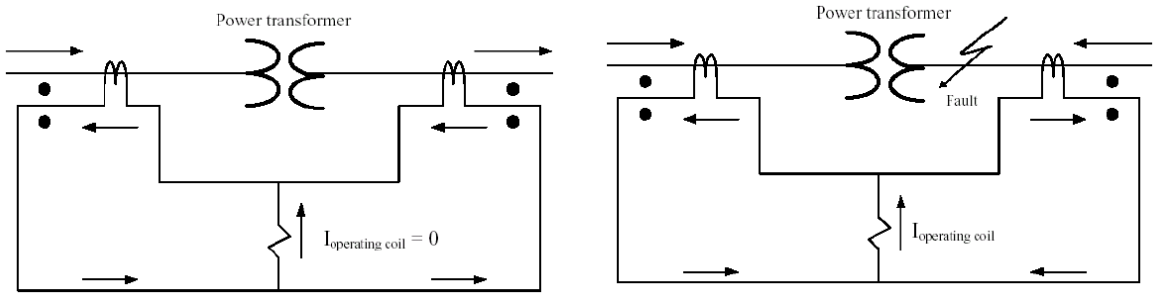

FIGURE 1. Basic differential scheme for (a) no-fault and (b) internal fault conditions of a power transformer

are not matched perfectly. This causes the differential signal to be considerably large even though there is no internal fault.

In order to prevent false tripping in these cases, in the literature for fault detection, several decision algorithms used for fault detection have been developed to be employed in the protective relay [2-16] but these several algorithms have different solutions and techniques. In [2], high frequency components of transformer terminal currents technique is proposed to detect internal faults in power transformers. The spectral energies of the transient currents are derived and used for discrimination. An application of a finite impulse response ANN (FIRANN) as differential protection for a three-phase power transformer is proposed in [3]. The networks have been designed to detect internal and external faults for primary and backup protection. In [4], a new algorithm based on processing differential current harmonics is proposed for digital differential protection of power transformers. This algorithm has been developed by considering different behaviors of second harmonic components of the differential currents under fault and inrush current conditions. In [5], a novel analysis of the currents arising during a turn-to-turn fault in transformer, in which a winding is delta-connected is done, so that data acquisition pre- and post-fault conditions may lead to a correct diagnosis. The approach given in this paper is based on the analysis of current sequences which appear in the fault state, and mainly in the nature of a zero sequence current (ZSC) in a delta winding, which is thoroughly discussed. In [6], the paper addresses turn-to-turn faults in power transformer windings. A sensitive detection method of these kinds of faults is presented.

In addition, wavelet transform has been reported in the literature [13-18]. The advantage of the wavelet transform is that the band of analysis can be fine adjusted so that high frequency components and low frequency components are detected precisely. Results from the wavelet transform are shown both in time domain and in frequency domain. The development of a wavelet–based scheme for distinguishing between transformer inrush currents and power system fault currents is presented in [14]. Wavelet transforms concept, feature extraction, and method of discrimination between transformer inrush and fault currents are described. The performance of the technique is verified from simulation of a 132/11 kV transformer, connected to a 132 kV power system. In addition, in some approaches, artificial neural network techniques have been proposed in the literature [17,19-21] to deal with the problems in power transformer protection.

As a result, most research works are interested in only the effects from magnetizing inrush current and the discrimination between magnetizing inrush current and internal faults [14,18,22-26], etc. [27-29]. Due to the fact that identifying types of internal fault and

locating the phase with fault appearance are as important as fault detection; therefore, this paper concentrates on the types of internal fault in the transformer winding in order to prevent false tripping and decrease duration time for analyzing the types of internal fault. To avoid the malfunction of the differential relay, the development of more sophisticated protection systems as well as fault diagnosis for the power transformer has been progressed with the applications of wavelet transform (WT) and artificial neural networks (ANNs). Nowadays, a back-propagation neural network has been used to solve almost all types of problems [30-33]. The activation function is a key factor in the artificial neural network structure. Back-propagation neural networks support a wide range of activation functions such as sigmoid function and linear function. The choice of activation function can change the behavior of the back-propagation neural network considerably. There is no theoretical reason for selecting a proper activation function. Hence, the objective of this paper is to consider studies of an appropriate activation function for identifying the types of fault including the phase with fault appearance of a two-winding three-phase power transformer using an application of Wavelet transform and a decision algorithm based on back propagation neural networks. The activation functions in each hidden layer and output layer are varied, and the results obtained from the decision algorithm are investigated. The transformer model with the stray capacitances is employed so that internal fault signals with high frequency components can be calculated. The simulations, analysis and diagnosis are performed using ATP/EMTP and MATLAB on a PC Pentium IV 2.4 GHz 512 MB. The current waveforms obtained from ATP/EMTP are extracted to several scales with the Wavelet transform, and the coefficients of the first scale from the Wavelet transformer are investigated. The comparison of the coefficients is performed and used as an input for training processes of the neural networks. The construction of the decision algorithm is detailed and implemented with various case studies based on Thailand electricity transmission and distribution systems.

2. Case Studies and Fault Detection Algorithms.

Artificial neural network requires fault signal samples from simulations to training and test processes but internal fault in transformer winding hardly occurs when comparison with fault in other equipments in power system, so various fault signals pattern will be obtained from simulation. The ATP/EMTP program is employed in simulating the transients of fault signals, at a sampling rate of 200 kHz. The present study is interested in identifying the types of internal fault in the transformer windings.

2.1. Transformer model using EMTP.

To study internal faults of the transformer, Bastard et al. [27] proposed modification of the BCTRAN subroutine. Normally, the BCTRAN uses a matrix of inductances with a size of 6×6 to represent a transformer, but with the internal fault conditions, the matrix is adjusted to be a size of 7×7 for winding to ground faults and of 8×8 for interturn faults. However, the effects of high frequency components which may occur during the faults are not included in such a model. In this paper, the combination of the transformer models proposed by Bastard et al. [27] with the high frequency model including capacitances of the transformer recommended by IEEE working group [34], is used for simulations of internal faults in the transformer windings.

The process for simulating internal faults based on the BCTRAN routine of EMTP can be summarized as follows:

1st step: Compute matrices $[R]$ and $[L]$ of the power transformer from manufacture test data [16,35] without considering the internal faults [27].

$$[R] = \begin{bmatrix} R_1 & \cdots & 0 \\ \vdots & \ddots & \vdots \\ 0 & \cdots & R_6 \end{bmatrix} \tag{1}$$

$$[L] = \begin{bmatrix} L_1 & L_{12} & \cdots & L_{16} \\ L_{21} & L_2 & \cdots & L_{26} \\ \vdots & \vdots & \ddots & \vdots \\ L_{61} & L_{62} & \cdots & L_6 \end{bmatrix} \tag{2}$$

2nd step: Modify Equations (1) and (2) to obtain the new internal winding fault matrices $[R]^*$ and $[L]^*$ as illustrated in Equations (3) and (4) [27].

$$[R]^* = \begin{bmatrix} R_a & 0 & 0 & 0 & 0 & 0 & 0 & 0 \\ 0 & R_b & 0 & 0 & 0 & 0 & 0 & 0 \\ 0 & 0 & R_c & 0 & 0 & 0 & 0 & 0 \\ 0 & 0 & 0 & R_2 & 0 & 0 & 0 & 0 \\ 0 & 0 & 0 & 0 & R_3 & 0 & 0 & 0 \\ 0 & 0 & 0 & 0 & 0 & R_4 & 0 & 0 \\ 0 & 0 & 0 & 0 & 0 & 0 & R_5 & 0 \\ 0 & 0 & 0 & 0 & 0 & 0 & 0 & R_6 \end{bmatrix} \tag{3}$$

$$[L]^* = \begin{bmatrix} L_a & M_{ab} & M_{ac} & M_{a2} & M_{a3} & M_{a4} & M_{a5} & M_{a6} \\ M_{ba} & L_b & M_{bc} & M_{b2} & M_{b3} & M_{b4} & M_{b5} & M_{b6} \\ M_{ca} & M_{cb} & L_c & M_{c2} & M_{c3} & M_{c4} & M_{c5} & M_{c6} \\ M_{2a} & M_{2b} & M_{2c} & L_2 & M_{23} & M_{24} & M_{25} & M_{26} \\ M_{3a} & M_{3b} & M_{3c} & M_{32} & L_3 & M_{34} & M_{35} & M_{36} \\ M_{4a} & M_{4b} & M_{4c} & M_{42} & M_{43} & L_4 & M_{45} & M_{46} \\ M_{5a} & M_{5b} & M_{5c} & M_{52} & M_{53} & M_{54} & L_5 & M_{56} \\ M_{6a} & M_{6b} & M_{6c} & M_{62} & M_{63} & M_{64} & M_{65} & L_6 \end{bmatrix} \tag{4}$$

3rd step: The inter-winding capacitances and earth capacitances of the HV and LV windings can be simulated by adding lumped capacitances connected to the terminals of the transformer as shown in Figure 2.

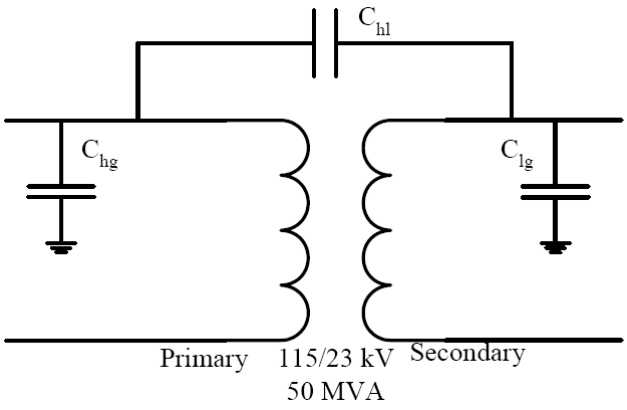

FIGURE 2. A two-winding transformer with the effects of stray capacitances [16]

2.2. **Winding to ground fault simulation.** A 50 MVA, 115/23 kV two-winding three-phase transformer is employed in simulations with all parameters and configuration provided by a manufacturer [16,35]. The scheme under investigations is a part of Thailand electricity transmission and distribution system as depicted in Figure 3.

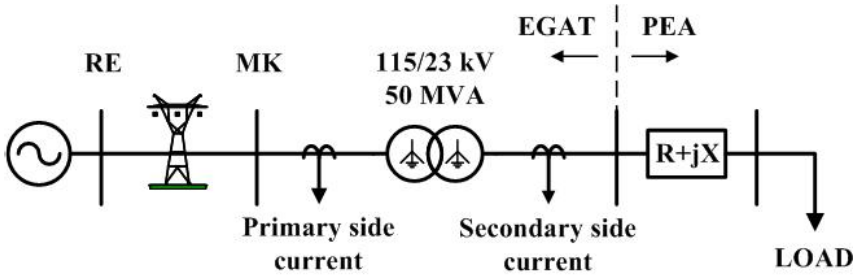

FIGURE 3. The system used in simulations studies [16]

From Figure 3, it can be seen that the transformer, which is a step down transformer is connected between two subtransmission sections. To implement the transformer model and cover all regions of operating conditions, training and testing data are simulated with various changes of system parameters as follows:

1) The angles on phase A voltage waveform for the instant of fault inception are 0°-330° (each step is 30°).

2) For the winding to ground faults, the fault positions as shown in Figure 4 are designated on any phases of the transformer windings (both primary and secondary) at the length of 10%, 20%, 30%, 40%, 50%, 60%, 70%, 80% and 90% measured from the line end of the windings.

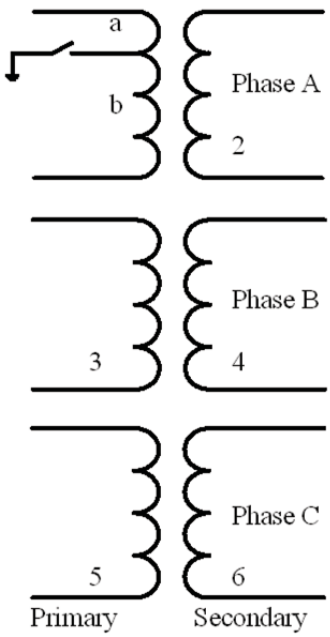

FIGURE 4. The modification on ATP/EMTP model for a three-phase transformer with winding to ground faults [27]

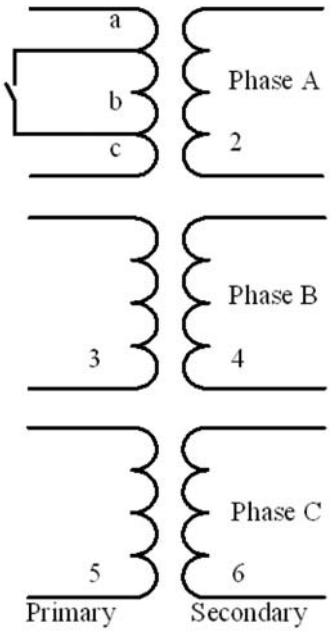

FIGURE 5. The modification on ATP/EMTP model for a three-phase transformer with interturn faults [27]

2.3. **Interturn fault simulation.** Interturn fault simulations are performed with various changes of system parameters as same as winding to ground fault simulations, but the position of fault that occurs is performed as follows:

1) For the interturn faults, the position of point a on the transformer winding, as shown in Figure 5, is varied at the length of 10%, 20%, 30%, 40%, 50%, 60%, 70% and 80% measured from the line end of the windings.

2) For the interturn faults, the position of point b on the transformer winding, as shown in Figure 5, is varied at the length of 10%, 20%, 30%, 40%, 50%, 60%, 70% and 80% measured from the line end of the windings.

3. **Fault Detection Decision Algorithm.** The primary and secondary current waveforms can be simulated using ATP/EMTP, and these waveforms are interfaced to MATLAB/Simulink for a construction of fault diagnosis process. The fault signals obtained in each phase from different currents of the transformer are illustrated in Figure 6(a) in which it shows phase A to ground fault occurred at high voltage winding. Figure 6(b) illustrates an example of phase A to ground fault occurred at low voltage winding. With fault signals obtained from the simulations, the differential currents, which are a deduction between the primary side current and the secondary side current in all three phases as well as the zero sequence, are calculated, and the resultant current signals are extracted using the discrete wavelet transform (DWT). The mother wavelet, daubechies4 (db4) [16], is employed to decompose high frequency components from the signals. The coefficients of the signals obtained from the DWT are squared for a more explicit comparison. Figure 7(a) illustrates an example of an extraction using DWT for the differential currents and zero sequence current from scale 1 to scale 5 for a case of phase A to ground fault at 10% of high voltage winding length while case of phase A to ground fault at 10% of low voltage winding length is shown in Figure 7(b).

In case of interturn fault, the primary and secondary current waveforms obtained when interturn phase A fault between 10% and 20% of high voltage winding length are shown in Figure 8(a) whereas case of interturn phase A fault between 10% and 20% of low voltage winding length is shown in Figure 8(b). Figure 9 illustrates examples of extraction processes using Wavelet transform for the differential currents and zero sequence current from scale 1 to scale 5 for a case of an interturn fault. The similarity between the fault

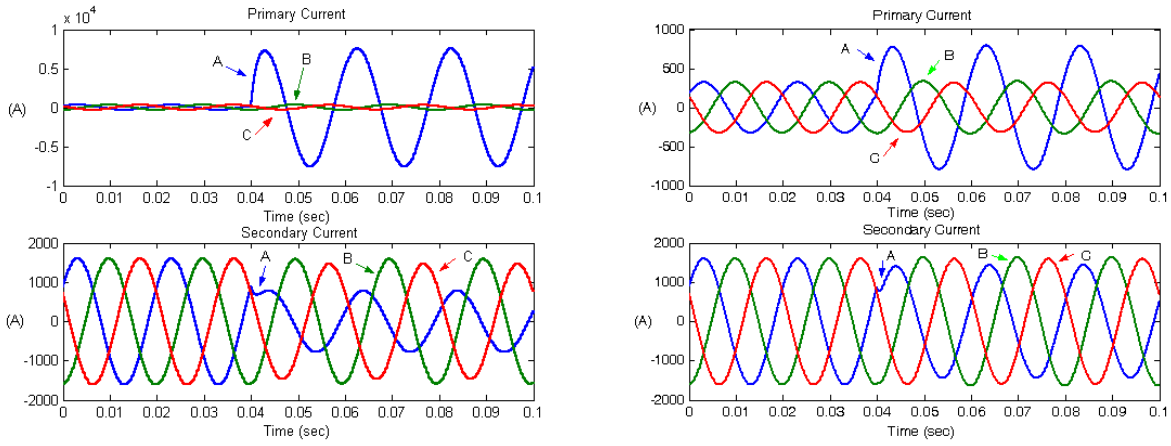

(a) Fault occurred at high voltage winding

(b) Fault occurred at low voltage winding

FIGURE 6. Primary and secondary currents for a case of phase A to ground fault at 10% in of winding length

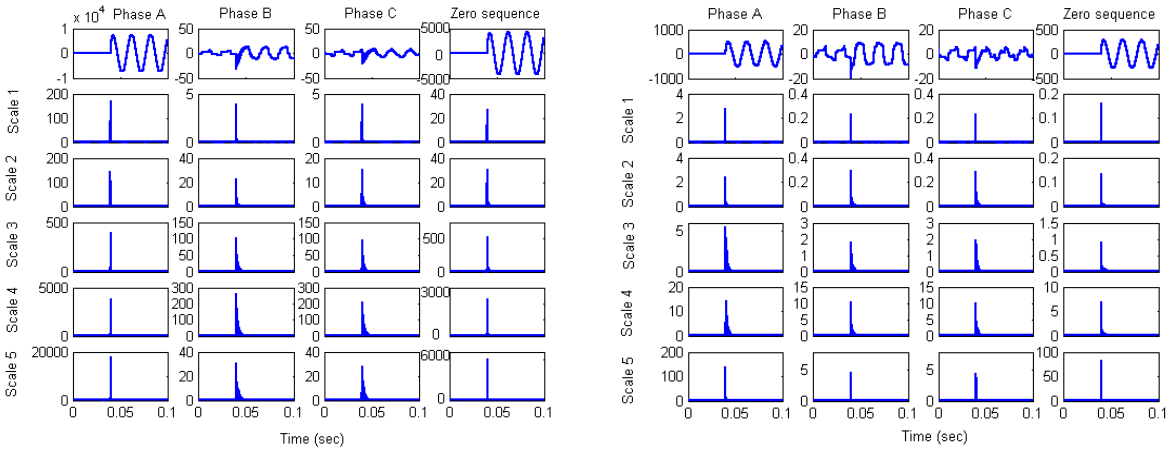

(a) Fault occurred at high voltage winding (b) Fault occurred at low voltage winding

FIGURE 7. Wavelet transform of differential currents (winding phase A to ground fault at 10% of winding length)

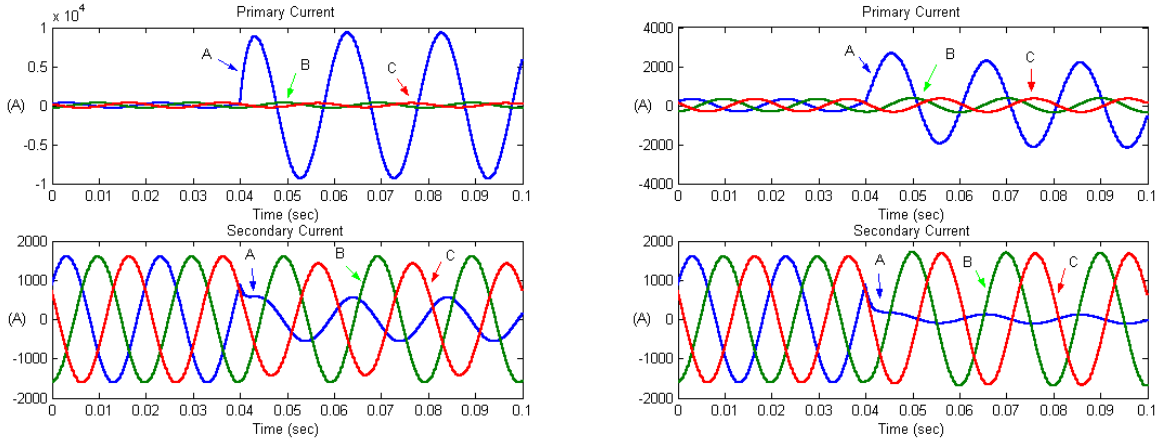

(a) Fault occurred at high voltage winding (b) Fault occurred at low voltage winding

FIGURE 8. Primary and secondary currents for a case of interturn phase A fault between 10% and 20% of winding length

signals waveforms from Figure 7 and Figure 8 can be seen obviously so that the comparison of the coefficients from each scale is considered as illustrated in Figure 10.

From Figure 10, DWT is applied to the quarter cycle of differential current waveforms after the fault inception. By performing many simulations [16], it has been found that the coefficient in scale 1 from DWT seems enough to indicate the fault inception. As a result, it is unnecessary to use other coefficients from higher scales in this algorithm, and the coefficients of scale 1 obtained using the DWT are used for training and test processes for the back-propagation neural network (BPNN).

4. **Neural Network Decision Algorithm and Simulation Results.** In this paper, a three-layer BPNN with one input layer, two hidden layers and one output layer is employed as illustrated in Figure 11. A training process is performed using neural network toolboxes in MATLAB. It can be divided into three parts as follows [36]:

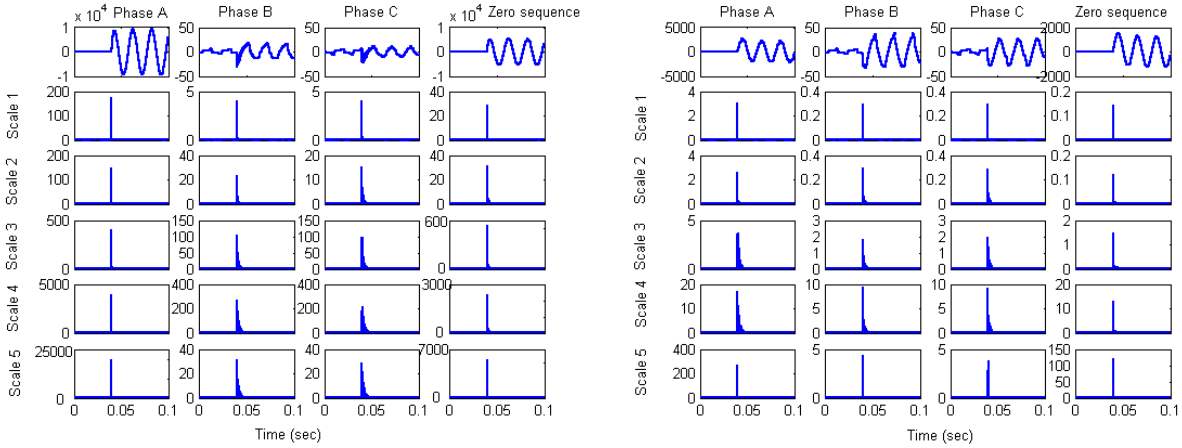

(a) Fault occurred at high voltage winding

(b) Fault occurred at low voltage winding

FIGURE 9. Wavelet transform of differential currents (interturn phase A fault between 10% and 20% of winding length)

1) The feedforward input pattern, which has a propagation of data from the input layer to the hidden layer and finally to the output layer for calculating responses from input patterns illustrated in Equations (5) and (6).

$$a^2 = f^2\left(lw^{2,1} * f^1\left(iw^{1,1} * p + b^1\right) + b^2\right), \tag{5}$$

$$o/p_{ANN} = f^3\left(lw^{3,2} * a^2 + b^3\right), \tag{6}$$

where,

p = input vector of BPNN;
$iw^{1,1}$ = weights between input and the first hidden layer;
$lw^{2,1}$ = weights between the first and the second hidden layers;
$lw^{3,2}$ = weights between the second hidden layer and output layers;
b^1, b^2 = bias in the first and the second hidden layers respectively;
b^3 = bias in output layers;
f^1, f^2 = activation function (Hyperbolic tangent sigmoid function: tanh);
f^3 = activation function (Linear function).

2) The back-propagation for the associated error between outputs of neural networks and target outputs. The error is fed to all neurons in the next lower layer, and also used to an adjustment of weights and bias.

3) The adjustment of the weights and bias by Levenberg-Marquardt (trainlm). This process is aimed at trying to match between the calculated outputs and the target outputs. Mean absolute percentage error (MAPE) as an index for efficiency determination of the BPNN is computed by using Equation (7).

$$MAPE = \frac{1}{n} * \sum_{i=1}^{n} \left| \frac{o/p_{ANNi} - o/p_{TARGETi}}{o/p_{TARGETi}} \right| * 100\% \tag{7}$$

where, n = number of test sets.

Before the training process, input data are normalized and divided into 1620 sets for training, and 810 sets for tests. A structure of the BPNN consists of 4 neuron inputs, two hidden layers and 8 neuron outputs. The inputs are the maximum coefficients details (cD1) in scale 1 at 1/4 cycle of phase A, B, C and zero sequence for post-fault differential currents as shown in Figure 12. The output variables of the neural networks are designated

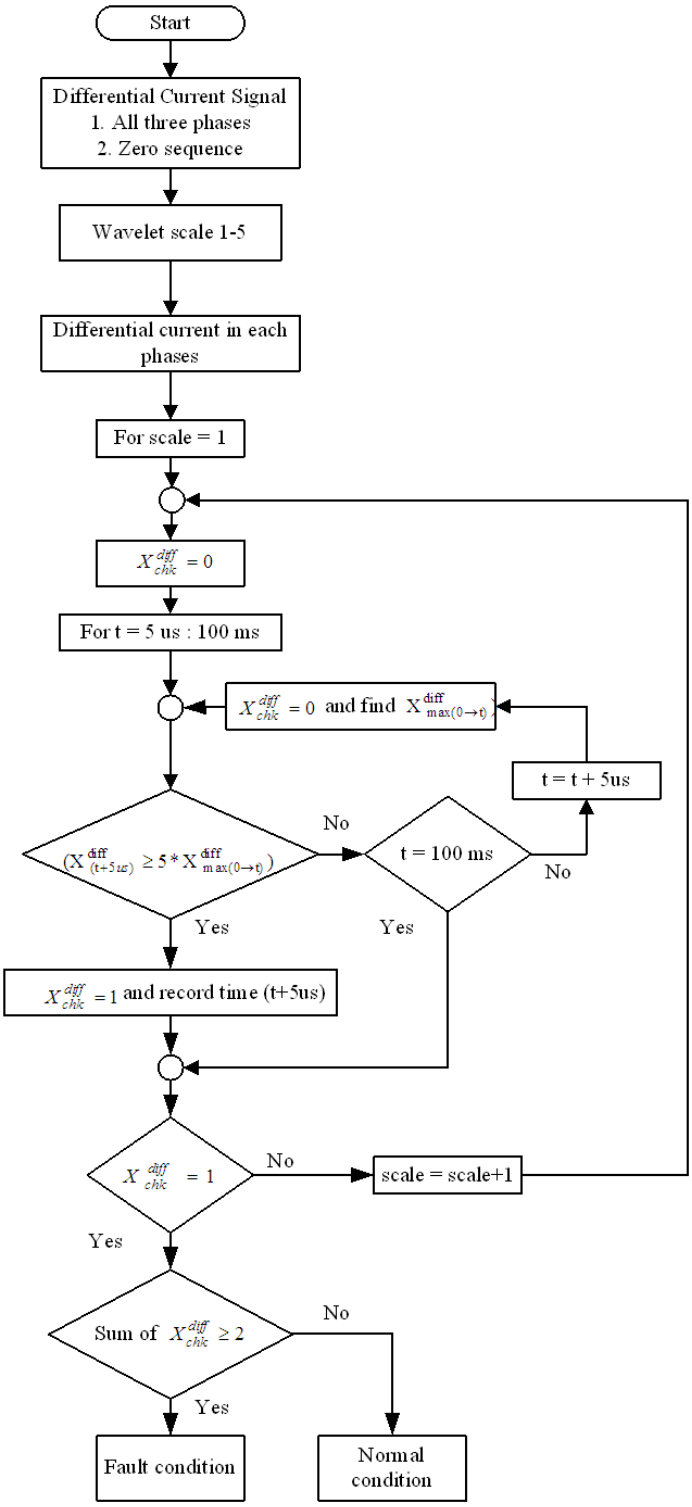

where,
scale = indicator scale of DWT, considered for detecting fault,
$X_{(t+5\mu s)}^{diff}$ = coefficient from DWT for the differential current detected from phase X at the time of t+5μs,
$X_{max(0\to t)}^{diff}$ = coefficient from DWT for the differential current detected from phase X at the time from t = 0 to t = t + 5μs,
X_{chk}^{diff} = comparison indicator for a change in coefficient from DWT (A_{check}^{diff}, B_{check}^{diff}, C_{check}^{diff}), used for separation between normal conditions and faults.

FIGURE 10. Flowchart for detecting the phase with a fault condition

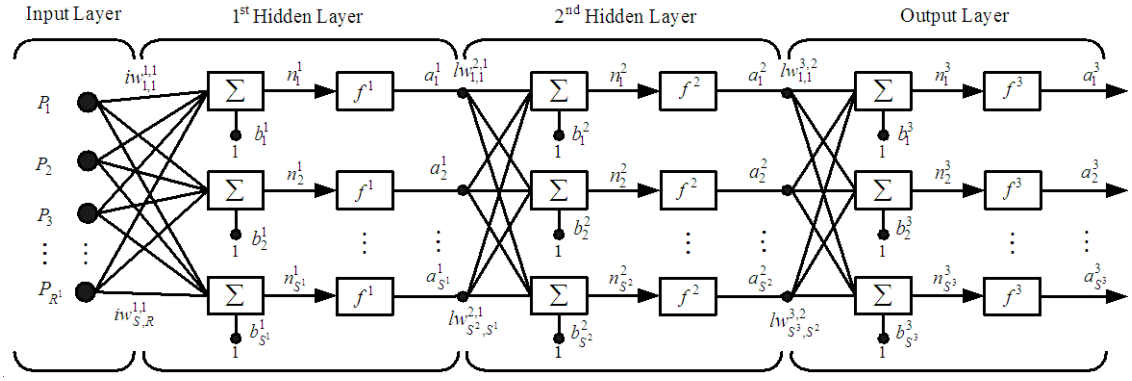

FIGURE 11. BPNN with two hidden layers [36]

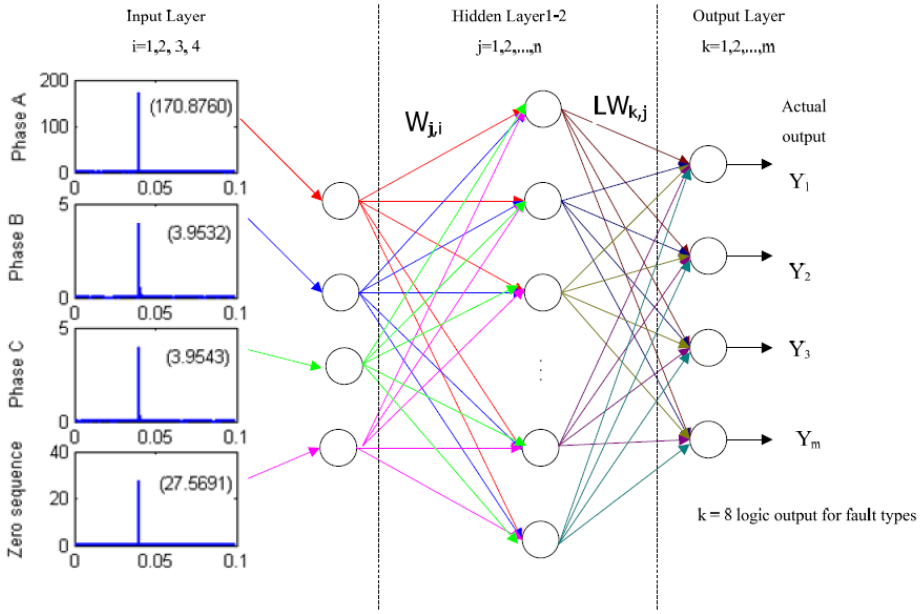

FIGURE 12. Magnitude in scale 1 for post-fault current signal shown in Figure 7(a)

as either 0 or 1 corresponding to phase A, B, C and ground (G) as presented in Table 1. If each output value of BPNN is less than 0.5, fault does not occur on each phase but if this output value of BPNN is more than 0.5, fault does occur. In addition, a number of neurons in both hidden layers are increased as well as varying the activation functions in all hidden layers and the output layer in order to select the best performance. In addition, the activation function is a key factor in the artificial neural network structure. The choice of activation function can change the behavior of the back-propagation neural network considerably. Hence, the activation functions in each hidden layers and output layer are varied as shown in Table 2 in order to select the best activation function for identifying internal fault types.

During the training process, the weight and biases are adjusted, and there are 20,000 iterations in order to compute the best value of MAPE. The number of neurons in both hidden layers is increased before repeating the cycle of the training process. The training procedure is stopped when reaching the final number of neurons for the first hidden layer or the MAPE of test sets is less than 0.5%. The training process can be summarized

TABLE 1. Output patterns from neural networks

Classification of Fault	A1	B1	C1	G1	A2	B2	C2	G2
Winding phase A to ground fault at high voltage winding (AGHV)	1	0	0	1	0	0	0	0
Winding phase A to ground fault at low voltage winding (AGLV)	0	0	0	0	1	0	0	1
Interturn phase A fault at high voltage winding (AHV)	1	0	0	0	0	0	0	0
Interturn phase A fault at low voltage winding (ALV)	0	0	0	0	1	0	0	0
Winding phase B to ground fault at high voltage winding (BGHV)	0	1	0	1	0	0	0	0
Winding phase B to ground fault at low voltage winding (BGLV)	0	0	0	0	0	1	0	1
Interturn phase B fault at high voltage winding (BHV)	0	1	0	0	0	0	0	0
Interturn phase B fault at low voltage winding (BLV)	0	0	0	0	0	1	0	0
Winding phase C to ground fault at high voltage winding (CGHV)	0	0	1	1	0	0	0	0
Winding phase C to ground fault at low voltage winding (CGLV)	0	0	0	0	0	0	1	1
Interturn phase C fault at high voltage winding (CHV)	0	0	1	0	0	0	0	0
Interturn phase C fault at low voltage winding (CLV)	0	0	0	0	0	0	1	0

TABLE 2. Activation functions in all hidden layers and output layers for training neural networks

Activation function in		
first hidden layer	second hidden layer	output layer
Hyperbolic Tangent sigmoid function	Logistic sigmoid function	Linear function
		Logistic sigmoid
		Hyperbolic Tangent sigmoid
	Hyperbolic Tangent sigmoid function	Linear function
		Logistic sigmoid
		Hyperbolic Tangent sigmoid
Logistic sigmoid function	Logistic sigmoid function	Linear function
		Logistic sigmoid
		Hyperbolic Tangent sigmoid
	Hyperbolic Tangent sigmoid function	Linear function
		Logistic sigmoid
		Hyperbolic Tangent sigmoid

as in a flowchart shown in Figure 13 while the results from the training process can be summarized in Figure 14.

From Figure 14, it can be seen that there are four cases of activation functions with average error less than 5% as follows:

1. Hyperbolic tangent – Logistic – Linear.
2. Hyperbolic tangent – Hyperbolic tangent – Linear.

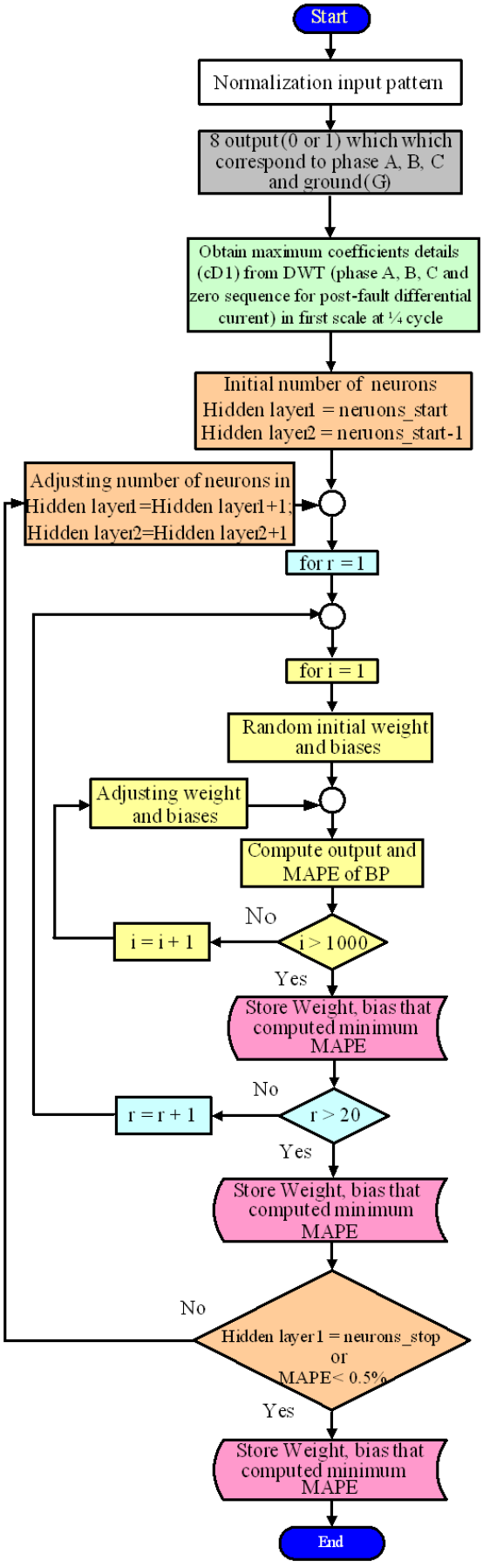

FIGURE 13. Flowchart for the training process

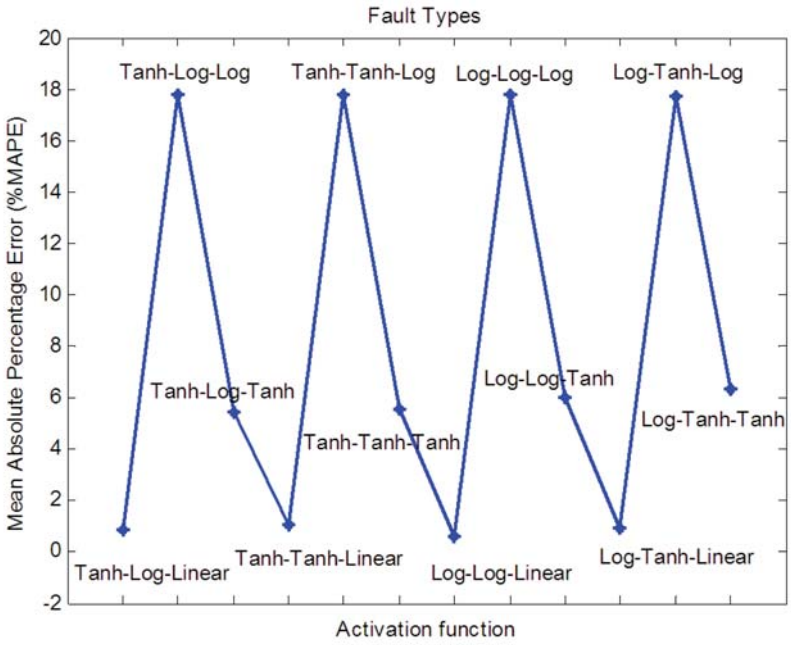

FIGURE 14. Comparison of MAPE for fault types at various activation functions

3. Logistic – Logistic – Linear.
4. Logistic – Hyperbolic tangent – Linear.

After training process, the decision algorithm is employed to identify the internal fault types in the transformer winding. Case studies are varied so that the algorithm capability can be verified. The system under consideration is shown in Figure 3. The total number of the case studies is 810. Case studies are performed with various types of fault at each position in the transformer including the variation of fault inception angles. The result obtained from various activation functions of case studies both high voltage and low voltage winding is shown in Table 3. From Figures 15-17, the comparison of average accuracy at various lengths of the winding among four cases of activation functions is shown while the average accuracy of various types of internal fault in each phase of high voltage winding and low voltage winding is shown in Figure 18. The results obtained from the algorithm proposed in this paper are shown in Table 3. It can be seen that Hyperbolic tangent – Hyperbolic tangent – Linear as activation function in each layer, is tested with various fault types on both high voltage and low voltage windings of the three-phase transformer. The average accuracy of fault types from the prediction of the decision algorithm is highly acceptable as illustrated in Figures 19-21.

TABLE 3. Average accuracy of case studies for identifying the types of internal fault

Activation function in			**Number of Case studies**	**Accuracy (%)**
the first hidden layer	**the second hidden layer**	**the output layer**		
Hyperbolic tangent sigmoid function	Logistic sigmoid function	Linear function	810	95.926
	Hyperbolic tangent sigmoid function	Linear function	810	96.914
Logistic sigmoid function	Logistic sigmoid function	Linear function	810	95.679
	Hyperbolic tangent sigmoid function	Linear function	810	96.543

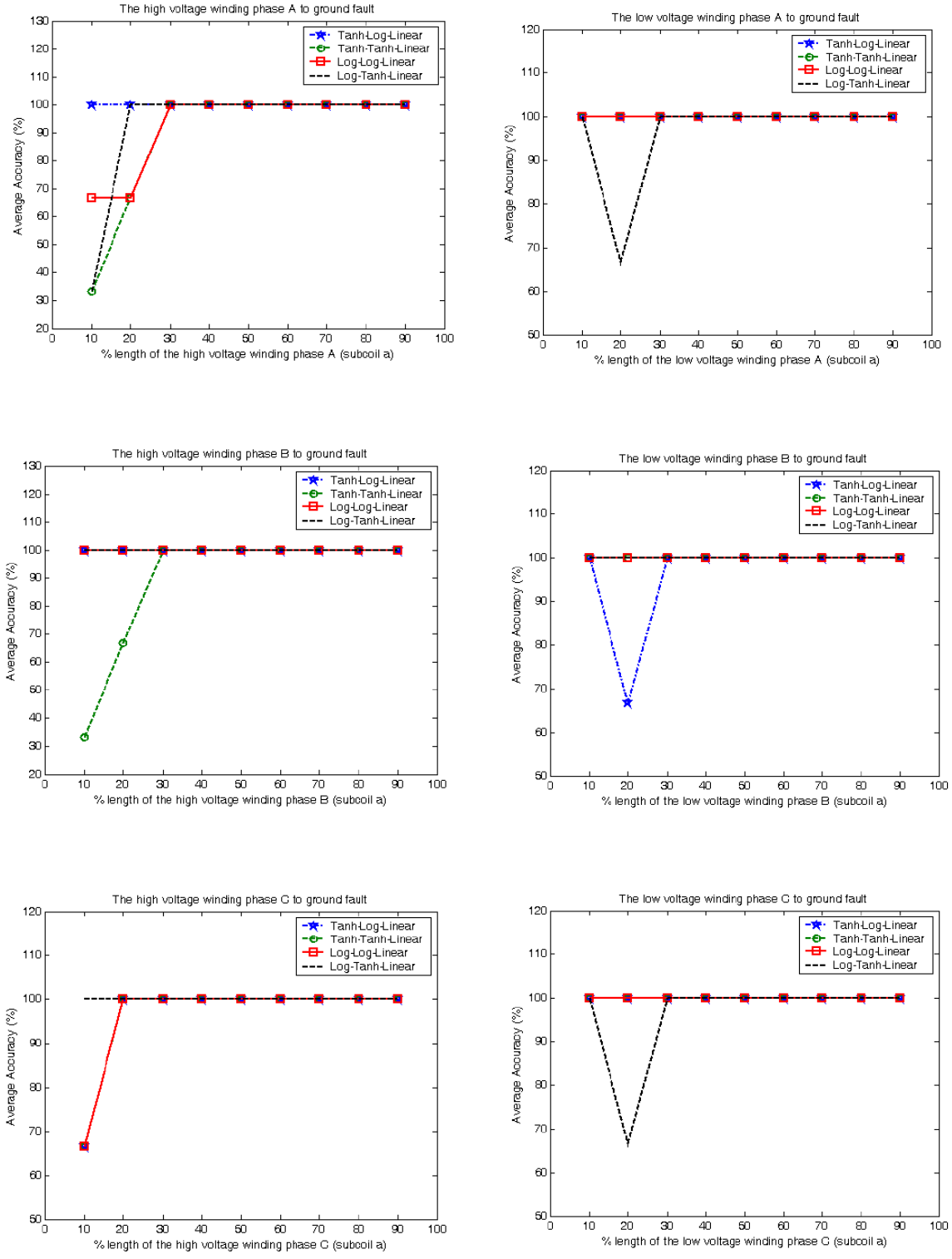

(a) High voltage (b) Low voltage

FIGURE 15. Comparison of average accuracy when identifying the winding to ground fault type at various lengths of the winding (subcoil a as shown in Figure 4) among various activation functions

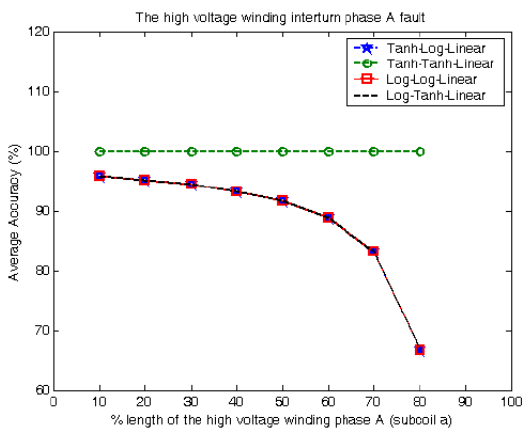

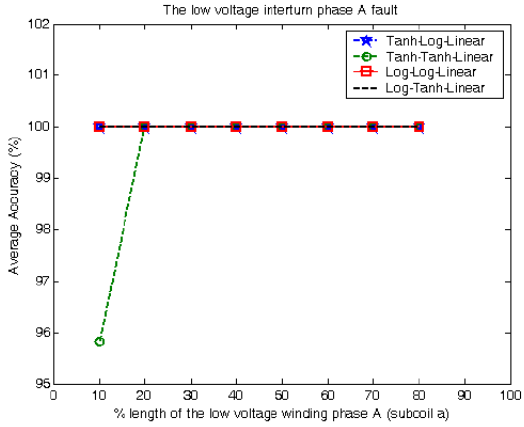

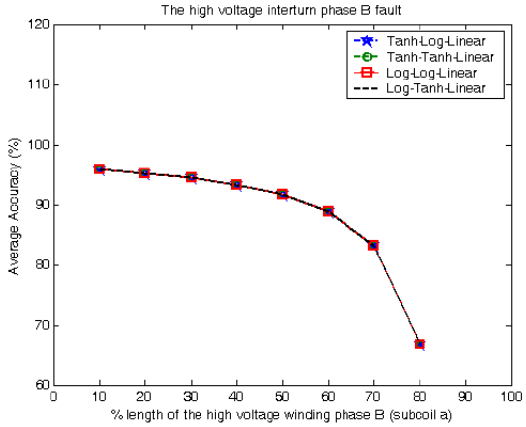

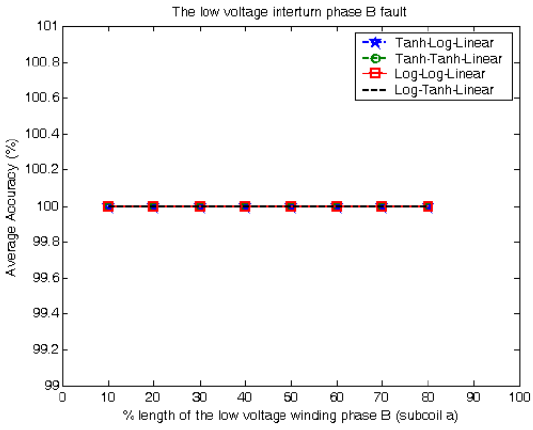

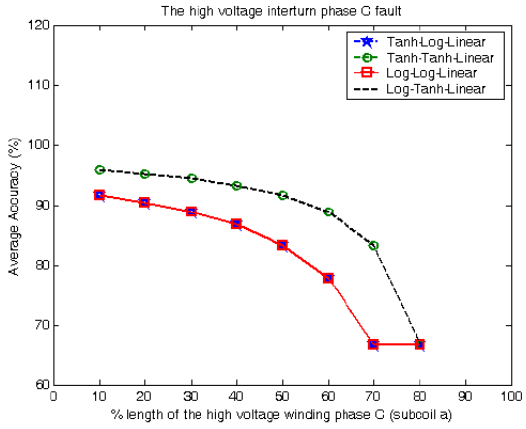

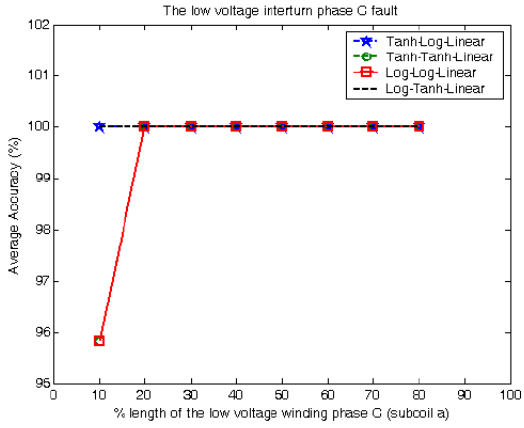

(a) High voltage (b) Low voltage

FIGURE 16. Comparison of average accuracy when identifying the interturn fault type at various lengths of the winding (subcoil a as shown in Figure 5) among various activation functions

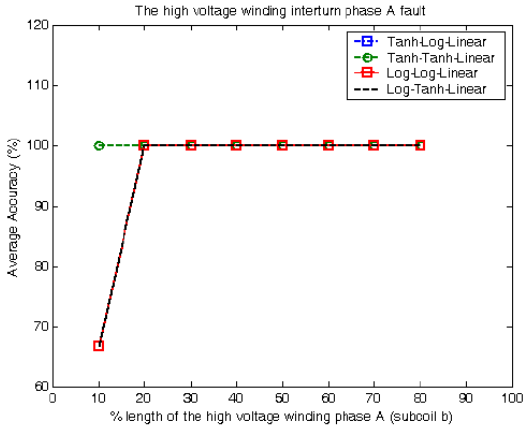

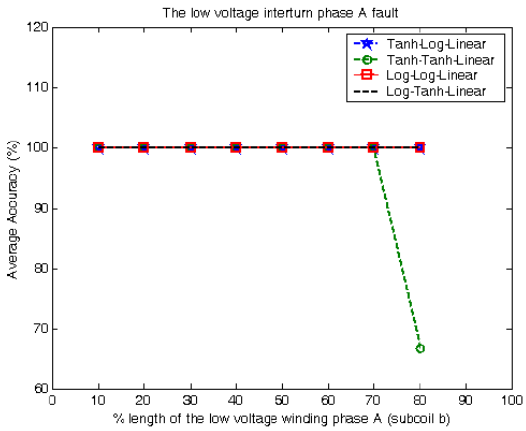

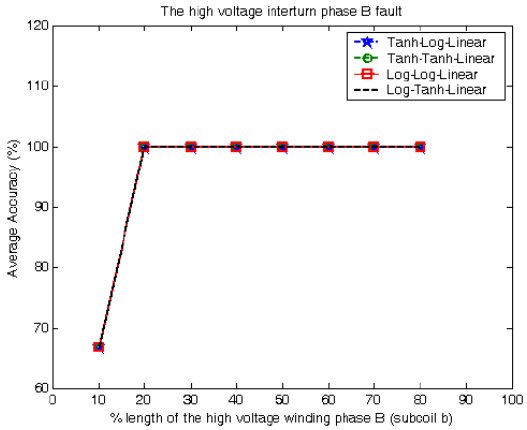

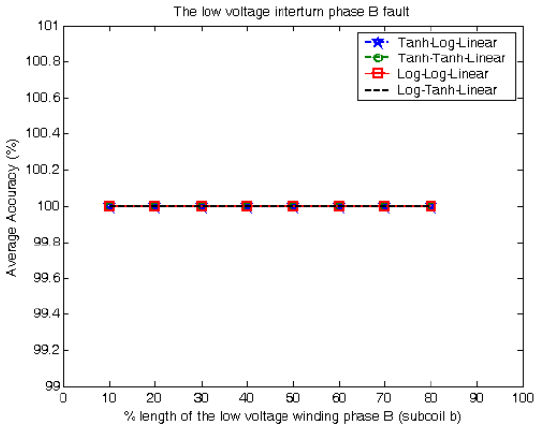

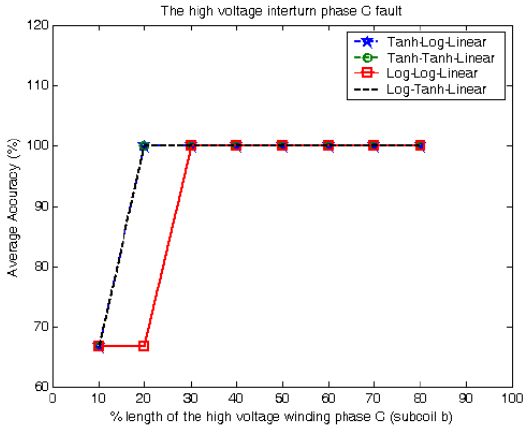

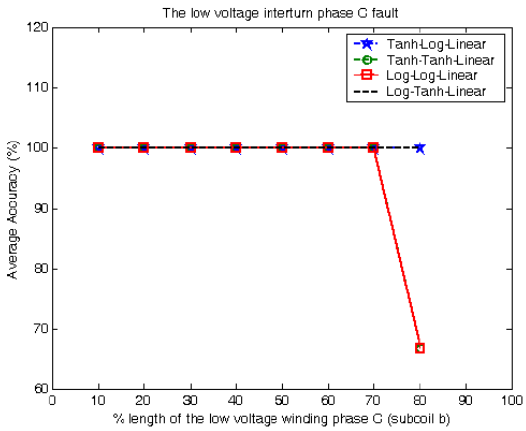

(a) High voltage (b) Low voltage

FIGURE 17. Comparison of average accuracy when identifying the interturn fault type at various lengths of the winding (subcoil b as shown in Figure 5) among various activation functions

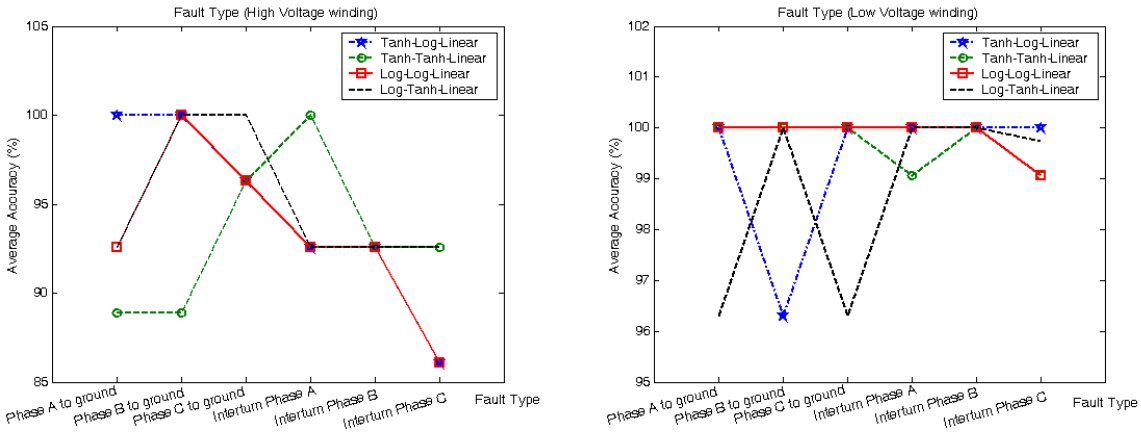

(a) High voltage (b) Low voltage

FIGURE 18. Comparison of average accuracy when identifying the types of internal fault among various activation functions

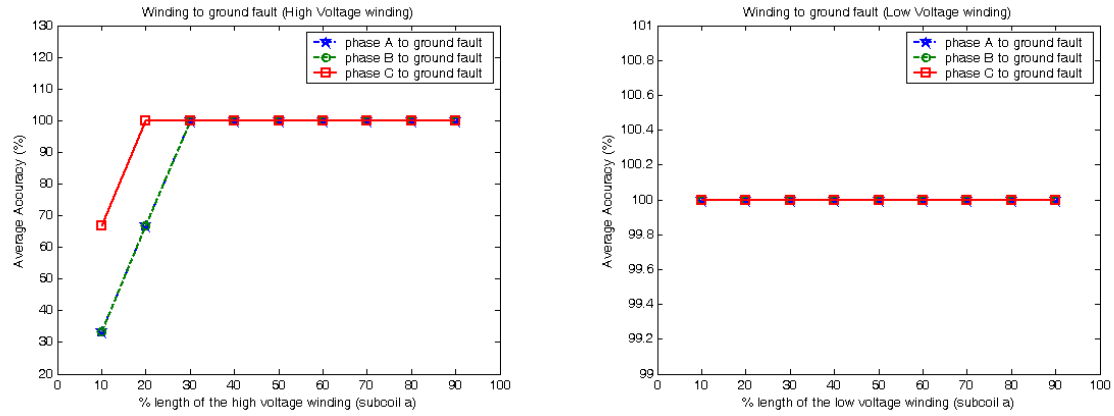

(a) High voltage (b) Low voltage

FIGURE 19. Comparison of average accuracy of winding to ground fault at various lengths of the winding (subcoil a as shown in Figure 4) among phase that fault occurs

5. **Conclusions.** In this paper, a decision algorithm using discrete wavelet transform in combination with back propagation neural networks to identify types of internal faults including locating the phase with fault appearance along the transformer windings has been proposed. The maximum coefficient from the first scale at 1/4 cycle of phase A, B, and C of post-fault differential current signals and zero sequence current obtained by the wavelet transform has been used as an input for the training process of a neural network in a decision algorithm with a use of the back propagation neural networks. Therefore, the activation functions in the all hidden layers and output layer have been varied. Various case studies have been carried out including the variation of fault inception angles, fault types, and fault locations. The results show that the proposed algorithm is able to locate the phase with fault appearance along the transformer windings with an accuracy of higher than 96% when employing hyperbolic tangent – hyperbolic tangent – linear as activation functions in each layer as summarized in Table 3. This technique would be useful in the differential protection scheme for the transformer.

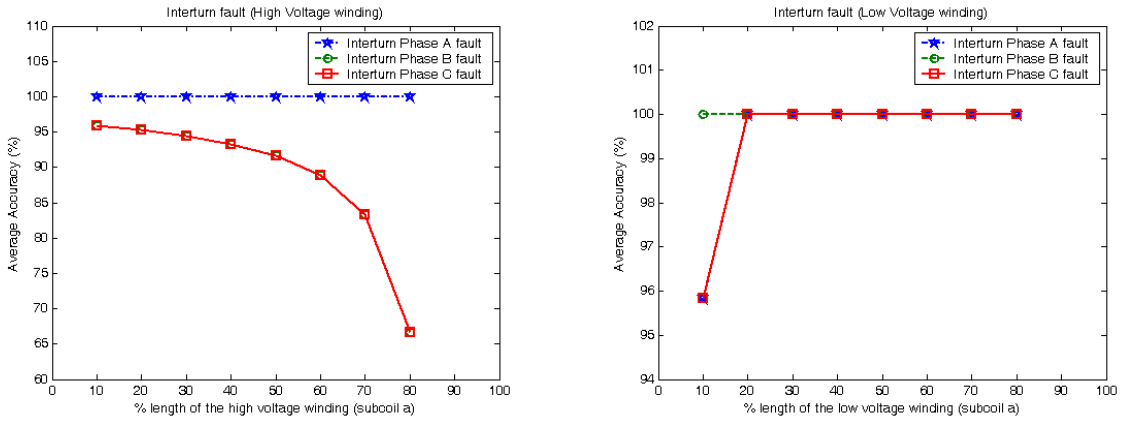

(a) High voltage (b) Low voltage

FIGURE 20. Comparison of average accuracy of interturn fault at various lengths of the winding (subcoil a as shown in Figure 5) among phase that fault occurs

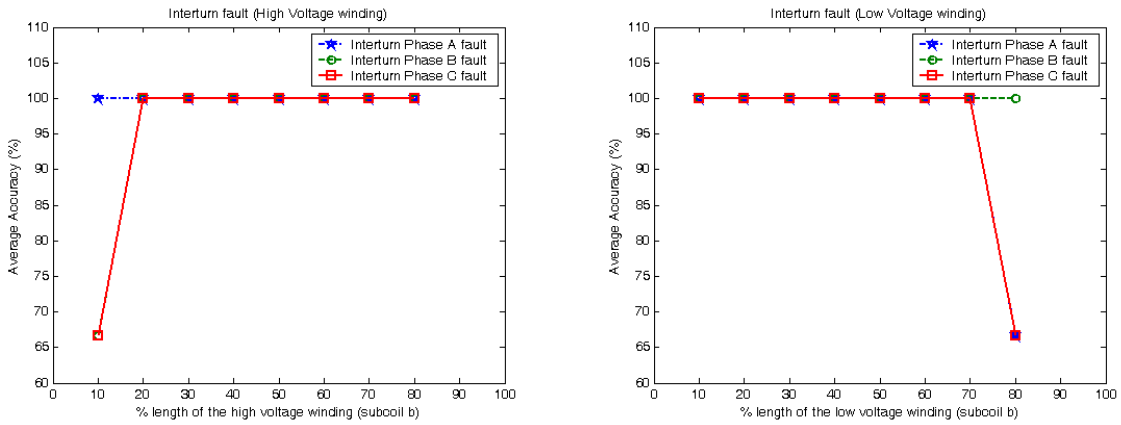

(a) High voltage (b) Low voltage

FIGURE 21. Comparison of average accuracy of interturn fault at various lengths of the winding (subcoil b as shown in Figure 5) among phase that fault occurs

Acknowledgment. This work is partially supported by the King Mongkut's Institute of Technology Ladkrabang Research fund. The authors would like to thank for this financial support. The authors would like also to gratefully acknowledge the helpful comments and suggestions of the reviewers, which have improved the presentation.

REFERENCES

[1] S. H. Horowitz and A. G. Phadke, *Power System Relaying*, John Wiley & Sons Inc., 1992.
[2] Z. Bo, G. Weller and T. Lomas, A new technique for transformer protection based on transient detection, *IEEE Trans. Power Delivery*, vol.15, no.4, pp.870-875, 2000.
[3] A. L. Orille-Fernandez, N. K. I. Ghonaim and J. A. Valencia, A FIRANN as a differential relay for three-phase power transformer protection, *IEEE Trans. on Power Delivery*, vol.16, no.2, pp.215-218, 2001.
[4] O. A. S. Youssef, Discrimination between faults and magnetizing inrush currents in transformers based on wavelet transforms, *Electric Power Systems Research*, vol.63, no.2, pp.87-94, 2002.

[5] M. E. H. Golshan, M. Saghaian-nejad, A. Saha and H. Samet, A new method for recognizing internal faults from inrush current conditions in digital differential protection of power transformers, *Electric Power Systems Research*, vol.71, no.1, pp.61-71, 2004.

[6] G. D. González, J. G.-A. Fernández and P. Arboleya, Diagnosis of a turn-to-turn short circuit in power transformers by means of zero sequence current analysis, *Electric Power Systems Research*, vol.69, no.2, pp.321-329, 2004.

[7] Z. Gajic, I. Brncic, F. Mekic, B. Hillström and I. Ivankovic, Sensitive turn-to-turn fault protection for power transformers, *Proc. of the 32nd Annual Western Protective Relay Conference*, 2005.

[8] V. Jeyabalan and S. Usa, Frequency domain correlation technique for PD location in transformer winding, *IEEE Transactions on Dielectrics and Electrical Insulation*, vol.16, no.4, pp.1160-1167, 2009.

[9] X. Lin, J. Huang, L. Zeng and Z. Bo, Analysis of electromagnetic transient and adaptability of second-harmonic restraint based differential protection of UHV power transformer, *IEEE Trans. on Power Delivery*, vol.25, no.4, pp.2299-2307, 2010.

[10] A. Akbari, A. Setayeshmehr, H. Borsi, E. Gockenbach and I. Fofana, Intelligent agent-based system using dissolved gas analysis to detect incipient faults in power transformers, *IEEE Electrical Insulation Magazine*, vol.26, no.6, pp.27-40, 2010.

[11] S. Singh and M. N. Bandyopadhyay, Dissolved gas analysis technique for incipient fault diagnosis in power transformers: A bibliographic survey, *IEEE Electrical Insulation Magazine*, vol.26, no.6, pp.41-46, 2010.

[12] Y. C. Kang, B. E. Lee, T. Y. Zheng, Y. H. Kim and P. A. Crossley, Protection, faulted phase and winding identification for the three-winding transformer using the increments of flux linkages, *IET Generation, Transmission & Distribution*, vol.4, no.9, pp.1060-1068, 2010.

[13] M. G. Morante and D. W. Nocoletti, A wavelet-based differential transformer protection, *IEEE Trans. on Power Delivery*, vol.14, no.4, pp.1352-1358, 1999.

[14] O. A. S. Youssef, A wavelet-base technique for discrimination between faults and magnetizing inrush currents in transformers, *IEEE Trans. on Power Delivery*, vol.18, no.1, pp.170-176, 2003.

[15] P. Purkait and S. Chakravorti, Wavelet transform-based impulse fault pattern recognition in distribution transformers, *IEEE Trans. on Power Delivery*, vol.18, no.4, pp.1588-1589, 2003.

[16] A. Ngaopitakkul, A. Kunakorn and I. Ngamroo, Discrimination between external short circuits and internal faults in transformer windings using discrete wavelet transforms, *Proc. of the 40th IEEE Industries Application Society Annual Conference*, vol.1, no.1, pp.448-452, 2005.

[17] W. Chen, C. Pan, Y. Yun and Y. Liu, Wavelet networks in power transformers diagnosis using dissolved gas analysis, *IEEE Trans. on Power Delivery*, vol.24, no.1, pp.187-194, 2009.

[18] A. M. Gaouda and M. M. A. Salama, DSP wavelet-based tool for monitoring transformer inrush currents and internal faults, *IEEE Trans. on Power Delivery*, vol.25, no.3, pp.1258-1267, 2010.

[19] K. Meng, Z. Y. Dong, D. H. Wang and K. P. Wong, A self-adaptive RBF neural network classifier for transformer fault analysis, *IEEE Trans. on Power Systems*, vol.25, no.3, pp.1350-1360, 2010.

[20] M. Tripathy, R. P. Maheshwari and H. K. Verma, Power transformer differential protection based on optimal probabilistic neural network, *IEEE Trans. on Power Delivery*, vol.25, no.1, pp.102-112, 2010.

[21] N. Perera and A. D. Rajapakse, Recognition of fault transients using a probabilistic neural-network classifier, *IEEE Trans. on Power Delivery*, vol.26, no.1, pp.410-419, 2011.

[22] H.-C. Seo, C.-H. Kim, S.-B. Rhee, J.-C. Kim and O.-B. Hyun, Superconducting fault current limiter application for reduction of the transformer inrush current: A decision scheme of the optimal insertion resistance, *IEEE Trans. on Applied Superconductivity*, vol.20, no.4, pp.2255-2264, 2010.

[23] J. Ma, Z. Wang, Q. Yang and Y. Liu, A two terminal network-based method for discrimination between internal faults and inrush currents, *IEEE Trans. on Power Delivery*, vol.25, no.3, pp.1599-1605, 2010.

[24] T. S. Sidhu and M. S. Sachdev, On-line identification of magnetizing inrush current and internal faults in three-phase transformers, *IEEE Trans. on Power Delivery*, vol.7, no.4, pp.1885-1891, 1992.

[25] N. Chiesa and H. K. Høidalen, Transformer model for inrush current calculations: Simulations, measurements and sensitivity analysis, *IEEE Trans. on Power Delivery*, vol.25, no.4, pp.2599-2608, 2010.

[26] N. Chiesa and H. K. Høidalen, Novel approach for reducing transformer inrush currents: Laboratory measurements, analytical interpretation and simulation studies, *IEEE Trans. on Power Delivery*, vol.25, no.4, pp.2609-2616, 2010.

[27] P. Bastard, P. Bertrand and M. Meunier, A transformer model for winding fault studies, *IEEE Trans. on Power Delivery*, vol.9, no.2, pp.690-699, 1994.
[28] G. Hoogendorp, M. Popov and L. van der Sluis, Application of hybrid modeling for calculating interturn voltages in transformer windings, *IEEE Trans. on Power Delivery*, vol.24, no.3, pp.1742-1744, 2009.
[29] L. M. R. Oliveira and A. J. M. Cardoso, A permeance-based transformer model and its application to winding interturn arcing fault studies, *IEEE Trans. on Power Delivery*, vol.25, no.3, pp.1589-1598, 2010.
[30] Y. E. Shao and B.-S. Hsu, Determining the contributors for a multivariate SPC chart signal using artificial neural networks and support vector machine, *International Journal of Innovative Computing, Information and Control*, vol.5, no.12(B), pp.4899-4906, 2009.
[31] T. Su, J. Jhang and C. Hou, A hybrid artificial neural networks and particle swarm optimization for function approximation, *International Journal of Innovative Computing, Information and Control*, vol.4, no.9, pp.2363-2374, 2008.
[32] C. He, H. Li, W. Yu, X. Liu, X. Liang and H. Peng, Prediction of density and mechanical properties in syntactic foam using artificial neural network, *ICIC Express Letters*, vol.4, no.6(B), pp.2383-2388, 2010.
[33] C. He, H. Li, B. Wang, W. Yu and X. Liang, Prediction of compressive yield load for metal hollow sphere with crack based on artificial neural network, *ICIC Express Letters*, vol.3, no.4(B), pp.1263-1268, 2009.
[34] IEEE working group 15.08.09, Modeling and analysis of system transients using digital programs, *IEEE PES Special Publication*, 1998.
[35] ABB Thailand, *Test Report, no.56039.*
[36] H. Demuth and M. Beale, *Neural Network Toolbox User's Guide*, The MathWorks, Inc., 2001.